AIP | Journal of Applied Physics

Analytical models of approximations for wave functions and energy dispersion in zigzag graphene nanoribbons

Mahdi Moradinasab, Hamed Nematian, Mahdi Pourfath, Morteza Fathipour, and Hans Kosina

Citation: J. Appl. Phys. **111**, 074318 (2012); doi: 10.1063/1.3702429
View online: http://dx.doi.org/10.1063/1.3702429
View Table of Contents: http://jap.aip.org/resource/1/JAPIAU/v111/i7
Published by the American Institute of Physics.

Analytical models of approximations for wave functions and energy dispersion in zigzag graphene nanoribbons

Mahdi Moradinasab,[1,2,a)] Hamed Nematian,[2,3] Mahdi Pourfath,[1,2] Morteza Fathipour,[1] and Hans Kosina[2]
[1]*School of Electrical and Computer Engineering, University of Tehran, North Kargar St., Tehran, Iran*
[2]*Institute for Microelectronics, Technische Universität Wien, Gußhausstraße 27-29/E360, Wien A-1040, Austria*
[3]*Department of Electronics, Science and Research Branch, Islamic Azad University, Tehran, Iran*

(Received 25 January 2012; accepted 28 February 2012; published online 12 April 2012)

In this work, we present analytical solutions for the wave functions and energy dispersion of zigzag graphene nanoribbons. A nearest neighbor tight-binding model is employed to describe the electronic band structure of graphene nanoribbons. However, an exact analytical solution for the dispersion relation and the wave functions of zigzag nanoribbons cannot be obtained. We propose two approximations of the discrete energies, which are valid for a wide range of nanoribbon indices. Employing these models, selection rules for optical transitions and optical properties of zigzag graphene nanoribbons are studied.
 [http://dx.doi.org/10.1063/1.3702429]

I. INTRODUCTION

Graphene, a one-atomic-layer carbon sheet with a honeycomb structure has received much attention over the past few years. An extraordinarily high carrier mobility of more than 2×10^5 cm^2/Vs (Refs. 1–3) makes graphene a major candidate for future electronic applications. Graphene is also regarded as a pivotal material in the emerging field of spin electronics, due to spin coherence even at room temperature.[4,5] One of the many interesting properties of Dirac electrons in graphene is the drastic change of the conductivity of graphene-based structures with the confinement of electrons. Structures that realize this behavior are carbon nanotubes (CNTs) and graphene nanoribbons (GNRs), which impose periodic and zero boundary conditions, respectively, on the transverse electron wave-vector. In CNT-based devices, control over the chirality and diameter and thus of the associated electronic bandgap remains a major technological problem. GNRs do not suffer this problem and thus are recognized as promising building blocks for nano-electronic devices.[6] GNRs with a width of smaller than 10 nm with ultrasmooth edges have been fabricated.[7] CNTs and GNRs are represented by a pair of indices (n and m) called the chiral vector. The edges of GNRs can significantly affect the electronic properties of the ribbon. In the electronic band structure of GNRs with zigzag edges (ZGNRs), a flat band, which corresponds to localized states at the edges, appears around the Fermi level.[8] However, such states do not appear in GNRs with armchair edges (AGNRs).[8] The energy band structure of AGNRs can be obtained by making the transverse wavenumber discrete, in accordance with the edge boundary condition, which is analogous to the case of carbon nanotubes, where periodic boundary conditions apply.[9] An analytical model for the dispersion relation and the wave functions of AGNRs is presented in Ref. 10. However, because in ZGNRs, the transverse wavenumber depends not only on the ribbon width, but also on the longitudinal wavenumber, the energy band structure cannot be obtained simply by slicing the bulk graphene band structure. Therefore, exact analytical models cannot be derived for ZGNRs.[9] In this work, we present two approximations for the wavenumber of ZGNRs, which result in simple analytical expressions for band structure and wave functions. We show that the analytical model is valid for a wide range of GNR indices.

The organization of this paper is as the following: In Sec. II, the electronic structure of ZGNRs is studied. The wavenumber approximations to reach analytical models for the dispersion relation and the wave function are derived in Sec. III. In Sec. IV, the models are employed to obtain optical transition rules and optical properties of ZGNRs. The two approximations used in our models and the obtained optical properties are discussed in Sec. V. Finally, Sec. VI provides concluding remarks.

II. ELECTRONIC STRUCTURE

The structure of graphene consists of two types of sublattices, A and B, see Fig. 1. In graphene, three σ bonds hybridize in an sp^2 configuration, whereas the other $2p_z$ orbital, which is perpendicular to the graphene layer, forms π covalent bonds. Each atom in an sp^2-coordination has three nearest neighbors, located $a_{cc} = 1.42$ Å away. It is well known that the electronic and optical properties of GNRs are mainly determined by the π electrons.[11]. To model these π electrons, a nearest neighbor tight-binding approximation has been widely used.[12,13] Based on this approximation, the Hamiltonian can be written as

$$H = t \sum_{\langle p,q \rangle} (|A_p\rangle\langle B_q| + |B_q\rangle\langle A_p|). \quad (1)$$

$|A_p\rangle$ and $|B_p\rangle$ are atomic wave functions of the $2p_z$ orbitals centered at lattice sites and are labeled as A_p and B_p, respectively, $\langle p, q\rangle$ represents pairs of nearest neighbor sites p and q, $t = \langle A_p|H|B_q\rangle \approx -2.7\ eV$ is the transfer integral, and the on-site potential is assumed to be zero.

a)moradinasab@iue.tuwien.ac.at.

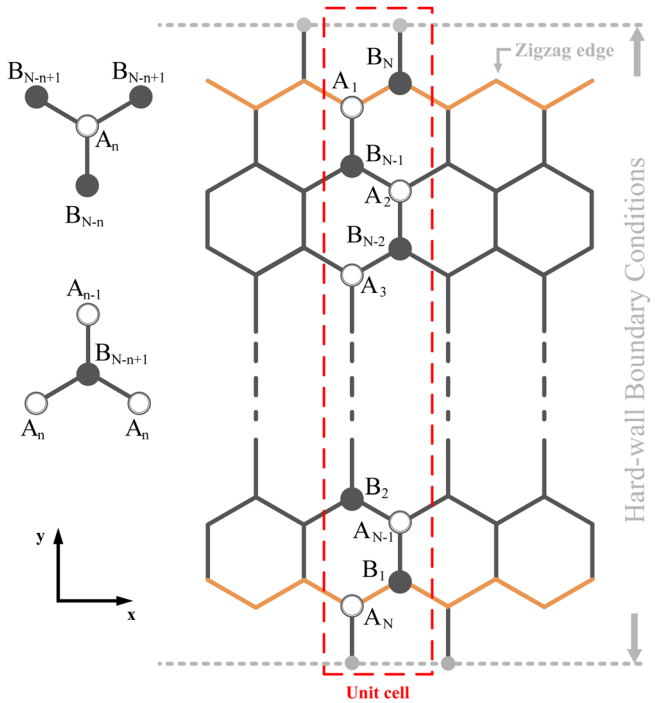

FIG. 1. The structure of a GNR with zigzag edges along the x direction. Each unit cell consists of N atoms at the sublattice A or B. A hard wall boundary condition is imposed on both edges.

The total wave function of the system is given by[14]

$$|\psi\rangle = C_A|\psi_A\rangle + C_B|\psi_B\rangle, \tag{2}$$

where $|\psi_A\rangle$ and $|\psi_B\rangle$ are the wave functions for sublattices A and B, respectively,

$$|\psi_A\rangle = \frac{1}{\sqrt{\Omega_A}}\sum_{p=1}^{N} e^{ik_x x_p^A}\phi_p^A|A_p\rangle, \quad |\psi_B\rangle = \frac{1}{\sqrt{\Omega_B}}\sum_{p=1}^{N} e^{ik_x x_p^B}\phi_p^B|B_p\rangle, \tag{3}$$

where $\Omega_{A/B}$ are the normalization factors, N is the number of atoms in the A and B sublattices in the unit-cell of the GNR, $x_p^{A/B}$ are the x-positions of the pth A/B-type carbon atoms, and $\phi_p^{A/B}$ is the amplitude of the transverse wave function of the pth A/B-type carbon atoms.

To obtain ϕ_p, one can substitute the ansatz for the wave functions into the Schrödinger equation. An A-type carbon atom at some atomic site n has one B-type atom at some atomic site $N-n$ and two B-type neighbors at $N-n+1$ (see Fig. 1),

$$\begin{cases} tf\ \phi_{N-n+1}^B + t\ \varphi_{N-n}^B = E\ \varphi_n^A, \\ t\ \varphi_{n-1}^A + tf\ \phi_n^A = E\ \varphi_{N-n+1}^B. \end{cases} \tag{4}$$

Replacing the index n with $n+1$ in the second relation of Eq. (4), one obtains

$$\phi_{N-n}^B = (1/E)(t\ \varphi_n^A + tf\ \phi_{n+1}^A). \tag{5}$$

Substituting this relation in Eq. (4), one can rewrite Eq. (4) as

$$C\phi_n^A = \phi_{n+1}^A + \phi_{n-1}^A, \tag{6}$$

with

$$C = \frac{(E/t)^2 - f^2 - 1}{f} \quad \text{and}$$
$$f = 2\cos(\boldsymbol{k}\cdot\boldsymbol{a}/2) = 2\cos\left(\frac{\sqrt{3}}{2}k_x a_{cc}\right). \tag{7}$$

Due to symmetry, a similar relation holds for the B-type carbon atoms,

$$C\phi_n^B = \phi_{n+1}^B + \phi_{n-1}^B. \tag{8}$$

Considering the boundary condition $\phi_0^A = \phi_0^B = 0$, the solution to the recursive formula is given by (see Appendix C)

$$\phi_n^B = \frac{\left(\frac{C+\sqrt{C^2-4}}{2}\right)^n - \left(\frac{C-\sqrt{C^2-4}}{2}\right)^n}{\sqrt{C^2-4}}\phi_1^B. \tag{9}$$

Depending on the values of C, Eq. (7) can have three different solutions. For $|C| > 2$, ϕ_n^B has a hyperbolic solution, where the wave function is localized at the edges of the ribbon,

$$\phi_n^B = \frac{2\sinh(n\theta)}{\sqrt{C^2-4}}\phi_1^B, \tag{10}$$

where θ is given by

$$C = 2\cosh(\theta). \tag{11}$$

For $C = \pm 2$, the amplitude of the wave function increases linearly with n. This critical case appears at the transition point from localized states to delocalized states. For $|C| < 2$, $\sqrt{C^2-4}$ is a pure imaginary number. The solution, ϕ_n^B, is therefore given by

$$\phi_n^B = \frac{\left(\frac{C+i\sqrt{4-C^2}}{2}\right)^n - \left(\frac{C-i\sqrt{4-C^2}}{2}\right)^n}{i\sqrt{4-C^2}}\phi_1^B, \tag{12}$$

$$\phi_n^B = \frac{2\sin(n\theta)}{\sqrt{4-C^2}}\phi_1^B = \frac{\sin(n\theta)}{\sin(\theta)}\phi_1^B, \tag{13}$$

where θ is the wavenumber and is given by

$$C = 2\cos(\theta). \tag{14}$$

Under this condition, the wave function has an oscillatory behavior and is not localized. The prefactors C_A and C_B in Eq. (2) are found to be $C_A = \pm C_B$ (see Appendix A). To simplify the equations, we assume $\phi_1^{A/B} = \sin(\theta)$. The resulting normalization factors can be obtained as $\Omega = N + 1/2$ (Appendix B), and the wave functions become

$$|\psi\rangle = \frac{1}{\sqrt{\Omega}}\sum_{n=1}^{N} e^{ik_x x_n^A}\sin(n\theta)|A_n\rangle \pm \frac{1}{\sqrt{\Omega}}\sum_{n=1}^{N} e^{ik_x x_n^B}\sin(n\theta)|B_n\rangle. \tag{15}$$

In order to obtain the respective energy spectrum, Eq. (7) can be written as

$$E = \pm t[Cf + f^2 + 1]^{1/2}. \tag{16}$$

By substituting Eq. (7) and Eq. (14) in Eq. (16), the energy dispersion relation takes the form

$$E = \pm t\left[1 + 4\cos^2\left(\frac{\sqrt{3}}{2}k_x a_{cc}\right) + 4\cos\left(\frac{\sqrt{3}}{2}k_x a_{cc}\right)\cos(\theta)\right]^{1/2}. \tag{17}$$

III. WAVENUMBER APPROXIMATIONS

In the following, the relation between θ and k_x is obtained. Setting $n = N+1$ in Eq. (4) gives

$$E\phi_0^B = t\phi_N^A + 2t\cos\left(\frac{\sqrt{3}}{2}k_x a_{cc}\right)\phi_{N+1}^A. \tag{18}$$

On the other hand, the wave functions for $n = N$ and $n = N+1$ are given by Eq. (13),

$$\phi_N^A = \frac{\sin(N\theta)}{\sin(\theta)}\phi_1^A, \quad \phi_{N+1}^A = \frac{\sin((N+1)\theta)}{\sin(\theta)}\phi_1^A. \tag{19}$$

By imposing a hardwall boundary condition, $\phi_0^B = 0$, Eq. (18) can be rewritten as

$$t\frac{\sin(N\theta)}{\sin(\theta)}\phi_1^A + 2t\cos\left(\frac{\sqrt{3}}{2}k_x a_{cc}\right)\frac{\sin((N+1)\theta)}{\sin(\theta)}\phi_1^A = 0, \tag{20}$$

and we obtain the quantization condition,

$$\frac{\sin(N\theta)}{\sin((N+1)\theta)} = -2\cos\left(\frac{\sqrt{3}}{2}k_x a_{cc}\right), \tag{21}$$

from Eq. (21). θ can be extracted and used in the analytical derivation of the wave functions and energy dispersion relation of ZGNRs. Figure 2 shows the variation of θ as a function of k_x for different subbands. As can be seen, a weak dependency exists between θ and k_x. However, we assume a constant θ with respect to k_x, so the right-hand side of Eq. (21) becomes a constant. At this point, two approaches exist to simplify Eq. (21) based on choosing k_x. In general, using all k_x in the range of $[0, \pi/\sqrt{3}a_{cc}]$, except $k_x = 2\pi/3\sqrt{3}a_{cc}$, results in non-analytical solution, and curve fitting is required to extract θ. This approach is first discussed. For $k_x = 0$, Eq. (21) can be written as

$$\frac{\sin(N\theta)}{\sin((N+1)\theta)} = -2. \tag{22}$$

Using curve fitting, one finds

$$\theta = \frac{Q}{N+P} = \begin{cases} Q = p_1\upsilon + p_2 \\ P = p_1'\upsilon + p_2', \end{cases} \tag{23}$$

where υ is related to the subband number q ($q = 2\upsilon$) and N is the index of ZGNR. p_1, p_2, p_1', and p_2' are fitting factors. Performing a fit for the range of $N \in [6, 100]$,

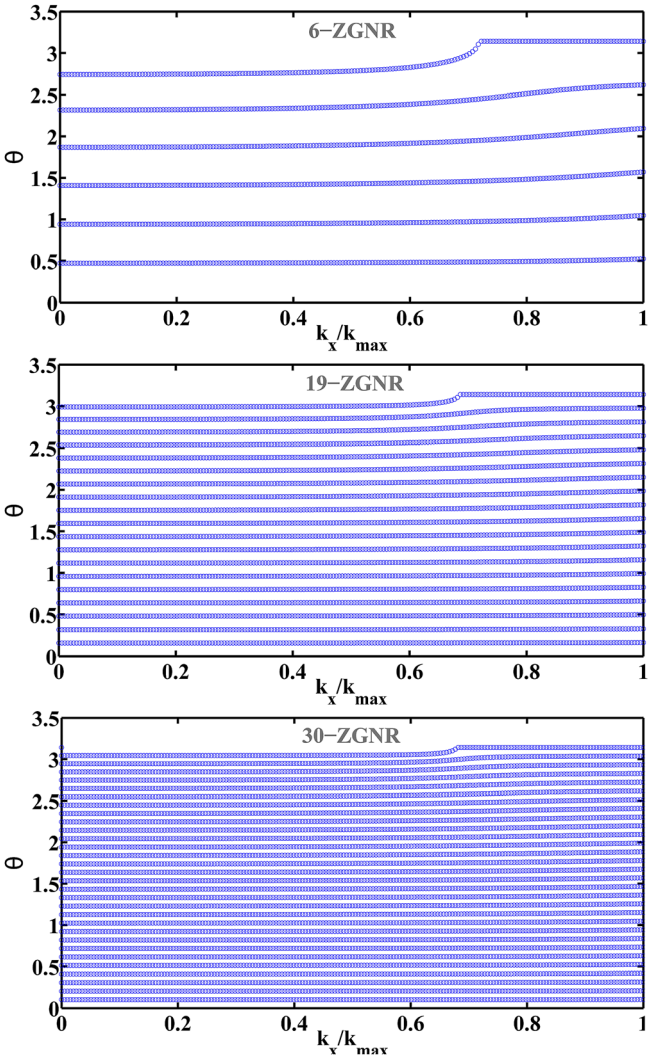

FIG. 2. Numerically evaluated wavenumber θ as a function of k_x for 6-ZGNR, 19-ZGNR, and 30-ZGNR.

$$\theta = \frac{3.31\upsilon - 0.5208}{N + 0.07003\upsilon + 0.5216}. \tag{24}$$

Figure 3 compares θ obtained from Eq. (24) with exact numerical results.

Another approach for approximating θ is selecting $k_x = 2\pi/3\sqrt{3}a_{cc}$, which makes the right side of Eq. (21) equal to -1,

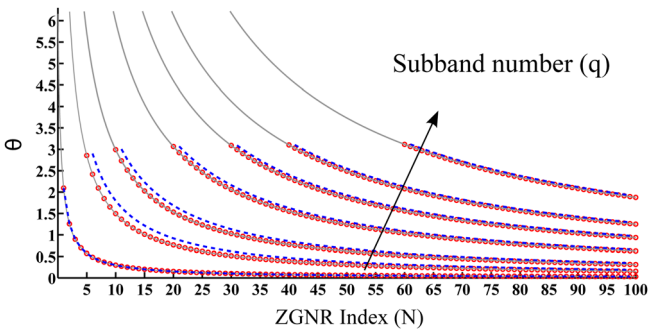

FIG. 3. The wavenumber θ as a function of the ribbon index, N, for different subband numbers, q. Dashed lines show the first approximation (Eq. (24)) and circles show the second approximation (Eq. (27)).

$$\sin(N\theta) + \sin((N+1)\theta) = 0,$$
$$2\sin((2N+1)\theta/2)\cos(\theta/2) = 0, \tag{25}$$

and has the following solution:

$$\theta = \frac{\upsilon\pi}{N+1/2}. \tag{26}$$

By representing υ in terms of subband index q, θ is obtained as a function of q and N,

$$\theta = \frac{q\pi}{2N+1}. \tag{27}$$

Figure 3 compares the discussed approximations with exact numerical results. The value of θ for Eq. (27) shows a good agreement with that obtained from numerical calculations. The approximation is valid for a wide range of ZGNR indices. Using the analytical expression for θ, analytical wave functions and energy dispersion are evaluated from Eq. (15) and Eq. (17). The results for a 6-ZGNR and a 19-ZGNR are shown in Fig. 4 and Fig. 5, respectively.

IV. OPTICAL MATRIX ELEMENTS AND TRANSITION RULES

Optical transition rules can be obtained from the optical matrix elements. The interband optical matrix element determines the probability for a transition from a state $|m\rangle$ to a final state $|n\rangle$ and is given by $(e/m_0)\langle n|\boldsymbol{A}\cdot\boldsymbol{p}|m\rangle$,[15] where e is the elementary charge, m_0 is the electron mass, $\boldsymbol{A} = A\hat{\boldsymbol{e}}$ is the vector potential, $\hat{e}$ is a unit vector parallel to $\boldsymbol{A}$, and $\boldsymbol{p}$ is the linear momentum operator. The vector potential can be separated from the expectation value, assuming the wave vector of the electromagnetic field is negligible compared to the electronic wave vector (dipole approximation). As a result, optical matrix elements can be achieved by evaluating momentum matrix elements, $\langle n|\hat{\boldsymbol{e}}\cdot\boldsymbol{p}|m\rangle$. In this work, the electromagnetic field is assumed to be polarized along the x direction.

$$p_{n,m} = \langle n|p_x|m\rangle. \tag{28}$$

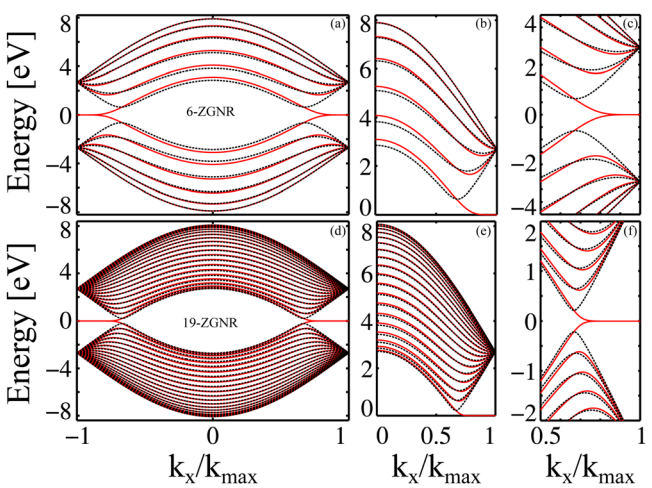

FIG. 4. The electronic band structure of 6-ZGNR ((a), (b), and (c)) and 19-ZGNR ((d), (e), and (f)). The analytical model (black dashed lines) is compared against the numerical results (red solid lines).

Knowing the wave function of atomic orbitals,[16] the matrix elements of the momentum operator can be calculated from Eq. (28). However, in most of the tight-binding models, the atomic orbitals are unknown, a difficulty which is usually circumvented by the gradient approximation.[17] By using the operator relation $\boldsymbol{p} = (im_0/\hbar)[H, \boldsymbol{r}]$, Eq. (28) can be rewritten as $p_{n,m} = (im_0/\hbar)\langle n|Hx - xH|m\rangle$. In this approximation, intra-atomic transitions are ignored. However, as we employ a single orbital model to describe the electronic band structure of ZGNRs, intra-atomic transitions are intrinsically neglected. Therefore, the momentum matrix elements can be approximated as[18]

$$p_{n,m} = (x_m - x_n)\frac{im_0}{\hbar}\langle n|H|m\rangle. \tag{29}$$

With the wave functions derived in Sec. II, evaluation of transition rules from Eq. (29) is possible. Using the wave functions from Eq. (15) in Eq. (29), and considering only nearest neighbors, one can obtain (see Appendix D)

$$P_{\theta,\theta'} = \frac{2\sqrt{3}m_0 a_{cc} t}{\hbar(2N+1)}\sin\left(\frac{\sqrt{3}}{2}ka_{cc}\right) \sum_{n=1}^{2N}\Big[\sin(n\theta')\sin((2N-n+1)\theta) - \sin(n\theta)\sin((2N-n+1)\theta')\Big]. \tag{30}$$

The upper limit of summation $2N$ is due to degenerate points of valance and conduction bands at $k_x = \pm 2\pi/3\sqrt{3}a_{cc}$. The subband indices are included in θ and θ' [see Eq. (27)]. The summation over sine functions in Eq. (30) determines the transition rules. By some trigonometric identities, one can rewrite this summation as follows:

$$P_{\theta,\theta'} = \frac{-2\sqrt{3}m_0 a_{cc} t}{\hbar(2N+1)}\sin\left(\frac{\sqrt{3}}{2}ka_{cc}\right) \left[\frac{\cos\left((2N+1)(\theta+\theta')/2\right)\sin\left(2N(\theta-\theta')/2\right)}{\sin\left((\theta-\theta')/2\right)} - \frac{\cos\left((2N+1)(\theta-\theta')/2\right)\sin\left(2N(\theta+\theta')/2\right)}{\sin\left((\theta+\theta')/2\right)}\right]. \tag{31}$$

Using the analytical approximation of θ in Eq. (27) for the cosine terms in Eq. (31) gives

$$\cos\left((2N+1)(\theta\pm\theta')/2\right) = \cos\left((q\pm q')\frac{\pi}{2}\right). \tag{32}$$

If $q = 2r+1$ and $q' = 2r'$ or $q = 2r$ and $q' = 2r'+1$, where r and r' are non-zero integers, $q \pm q' = 2r'' + 1$, both terms in the bracket of Eq. (31) will be zero. In the case of $q = 2r$ and $q' = 2r'$ or $q = 2r+1$ and $q' = 2r'+1$, the terms in the bracket will be non-zero. Therefore, the transitions between valence and conduction subbands only with the same parity (odd to odd and even to even) are allowed,

$$P_{\theta,\theta'} = P_{q,q'} = \begin{cases} 0, & \text{if } q = \text{odd (even) and } q' = \text{even (odd)}, \\ \neq 0, & \text{if } q = \text{odd (even) and } q' = \text{odd (even)}. \end{cases} \tag{33}$$

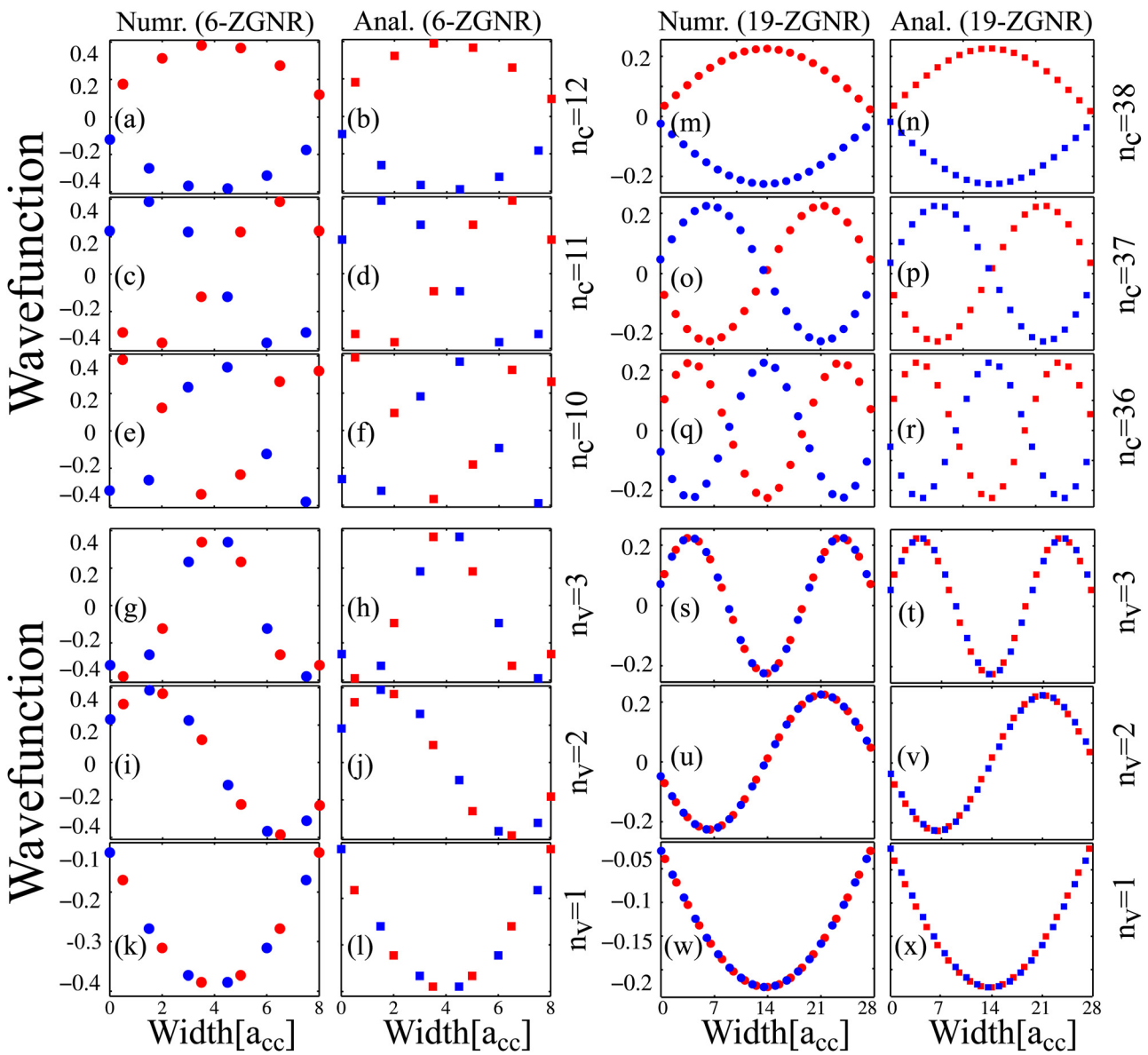

FIG. 5. The wave functions of 6-ZGNR and 19-ZGNR. Red(blue) symbols denote the wave functions in sublattice $B(A)$. The analytical model (squares) is compared against the numerical results (circles).

V. RESULTS AND DISCUSSION

In this section, the energy dispersion relation and the wave functions for the approximated discrete wavenumbers θ are evaluated and compared against exact numerical calculations.

Equation (27) is employed to give the wave functions and energy dispersions from Eq. (15) and Eq. (17), respectively. Based on the structure depicted in Fig. 1, the width of a zigzag nanoribbon is given by

$$W = \left(\frac{3N}{2} + 1\right) a_{cc}, \tag{34}$$

where $a_{cc} = 1.42$ Å is the carbon-carbon bond length in graphene. For ZGNRs with a width below 50 nm, indices in the range 6 to 235 have to be considered. In this range of indices, the wave functions and the energy dispersion have been evaluated. It should be noted that structures wider than 50 nm are also evaluated, and the results show excellent agreement with those obtained from numerical simulation. Figure 6 shows several wave functions for 125-ZGNR evaluated from two approximations proposed. As can be seen, the wave functions obtained by Eq. (27) are matched very well with the numerical calculations. The dispersion relation of some subbands for 125-ZGNR is shown in Fig. 7. Similar to the wave functions, the dispersion relations obtained by θ from Eq. (27) show well agreement with the numerical results.

An important conclusion that one can draw from these results is that the analytical approximation of θ presented in Eq. (27) is more accurate than the solution obtained by using a curve fitted θ (see Fig. 6 and Fig. 7). Also, the accuracy of the analytical method increases as the ZGNR index increases (see the energy dispersions for 6-ZGNR and 19-ZGNR in Fig. 4 and 125-ZGNR in Fig. 7). As can be seen in Fig. 2, this increase in accuracy is due to the fact that θ is relatively independent of changes in the wave-vector (k_x) for large values of N. In order to investigate the applicability of the

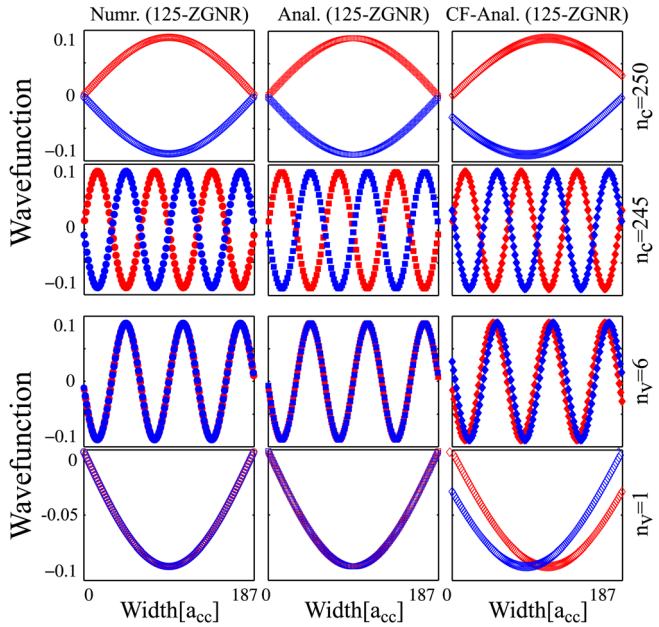

FIG. 6. The wave functions of 125-ZGNR. Red(blue) symbols denote the wave functions at the sublattice $B(A)$. The analytical model (squares) and curve-fitted model (diamonds) are compared against the numerical results (circles) for different subbands.

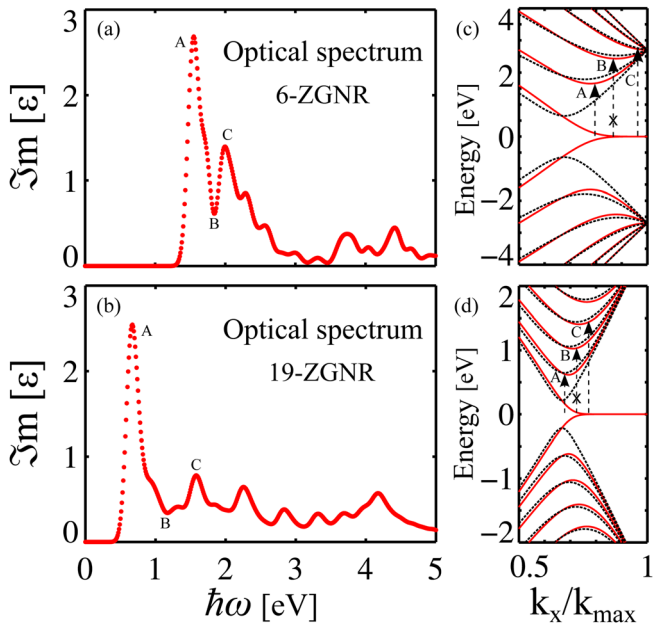

FIG. 8. Dielectric function of (a) 6-ZGNR and (b) 19-ZGNR. The peaks are related to electronic band structure of (c) 6-ZGNR and (d) 19-ZGNR.

proposed models, the optical matrix elements are derived analytically based on our models in Sec. IV. To evaluate the transition rules, we can also investigate the symmetry of the transition matrix element in Eq. (28). If the symmetry of this element spans the totally symmetric representation of the point group to which the unit cell belongs, then its value is not zero and the transition is allowed. Otherwise, the transition is forbidden. Assuming a uniform potential profile across the ribbon's width, the subbands' wave functions are either symmetric or antisymmetric along the y direction,

$$\langle -y|\psi_{c/v}\rangle = \pm\langle y|\psi_{c/v}\rangle. \tag{35}$$

Considering the wave functions for 6-ZGNR and 19-ZGNR (Fig. 5), subbands corresponding to odd indices are symmetric, while those corresponding to even indices are antisymmetric.

Therefore, the momentum matrix elements are non-zero for transitions from the symmetric (antisymmetric) to the symmetric (antisymmetric) wave functions. This transition rule results in transitions from subbands with odd (even) to odd (even) indices in ZGNRs,[19] which confirms the result obtained from our analytical derivation of the wave functions and momentum matrix elements.

The imaginary part of the dielectric function is used to investigate the optical properties of a material.[15] If the incident light is assumed to be polarized along the transport direction (x-axis), the imaginary part of the dielectric function in the linear response regime is given by[15]

$$\varepsilon_i(\omega) = \frac{1}{4\pi\varepsilon_0}\left(\frac{2\pi e}{m\omega}\right)^2 \times \sum_{k_x} |p_{c,v}|^2 \delta(E_c(k_x) - E_v(k_x) - \hbar\omega), \tag{36}$$

where $\hbar\omega$ is the energy of the incident photons and $p_{c,v}$ are the momentum matrix elements for optical transitions ($P_{\theta,\theta'}$ in our study). To demonstrate the applicability of our models, the imaginary part of the dielectric function ε_i is calculated numerically for 6-ZGNR and 19-ZGNR [see Fig. 8(a) and Fig. 8(b)]. Peaks in $\varepsilon_i(\omega)$ indicate absorptions of photons with energy $\hbar\omega$. From the electronic band structure in Fig. 8(c), it can be found that the peaks in $\varepsilon_i(\omega)$ are related to transitions from $n=6$ to $n=8$ (A) and $n=6$ to $n=10$ (C).

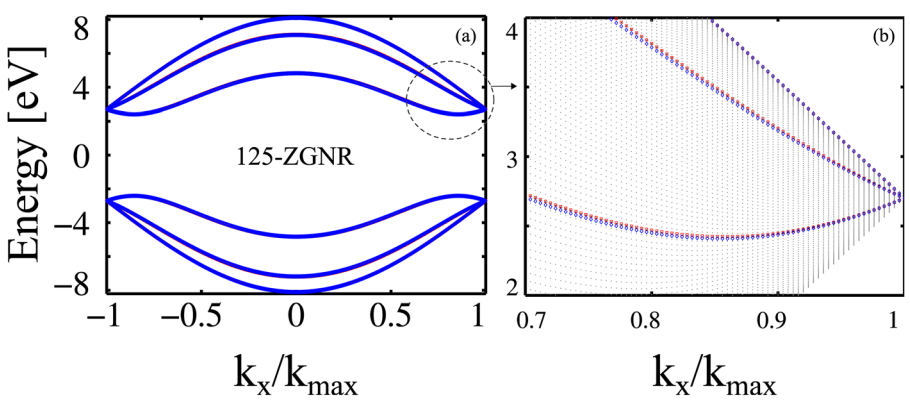

FIG. 7. The electronic band structure of 125-ZGNR. The analytical model (red symbols) and the curve fitted (blue symbols) are compared with the numerical results (black symbols).

The minimum designated as (B) is related to the transition from $n=6$ to $n=9$, which is forbidden according to the obtained transition rules. The same analysis exists for 19-ZGNR [see Fig. 8(b) and Fig. 8(d)]. Therefore, the allowed transitions are from odd to odd and even to even subband numbers, which is in agreement with our analytical derivation.

VI. CONCLUSIONS

We presented two methods for analytical approximation of the discrete energies in ZGNRs. Relations for the wave functions and the energy dispersion show good agreement with those obtained from numerical calculations. Our simple approximation is applicable for a wide range of ZGNR indices from N = 6 to N = 500. While the results show good agreement for small N-ZGNRs, the accuracy increases for wider ZGNRs. The analytical approach presented here is used to drive transition rules. Our model shows that transitions from odd to odd and even to even subband numbers are allowed and that other transitions are forbidden in ZGNRs. The model is applicable for the evaluation of optical properties of ZGNRs, such as dielectric response, absorption coefficient, and energy loss spectrum.

ACKNOWLEDGMENT

This work, as part of the ESF EUROCORES program EuroGRAPHENE, is partly supported by funds from FWF, contract I420-N16.

APPENDIX A: CALCULATION OF PREFACTORS

To obtain C_A and C_B in Eq. (2), one can substitute Eq. (1) and Eq. (3) into the Shrödinger equation $H|\psi\rangle = E|\psi\rangle$. Considering an A-type carbon atom at some atomic site, n, and its three nearest neighbors, the Hamiltonian can be written as

$$H = t|B_{N-n+1}\rangle\langle A_n| + t|B'_{N-n+1}\rangle\langle A_n| + t|B_{N-n}\rangle\langle A_n|. \quad \text{(A1)}$$

Using Eq. (A1) along with the wave functions obtained in Eq. (15), one obtains

$$\begin{aligned} EC_A e^{ik_x x_n^A}\sin(n\theta) &= tC_B e^{ik_x x_{N-n+1}^B}\sin((N-n+1)\theta) \\ &+ tC_B e^{ik_x x_{N-n+1}^{B'}}\sin((N-n+1)\theta) \\ &+ tC_B e^{ik_x x_{N-n}^B}\sin((N-n)\theta). \end{aligned} \quad \text{(A2)}$$

Therefore, the relation between C_A and C_B can be written as

$$\begin{aligned} EC_A\sin(n\theta) &= tC_B\left[\left(e^{ik_x(x_{N-n+1}^B - x_n^A)} + e^{ik_x(x_{N-n+1}^{B'} - x_n^A)}\right)\right. \\ &\left.\sin((N-n+1)\theta) + e^{ik_x(x_{N-n}^B - x_n^A)}\sin((N-n)\theta)\right] \\ &= tC_B\left[2\cos\left(\frac{\sqrt{3}}{2}k_x a_{cc}\right)\sin((N-n+1)\theta)\right. \\ &\left.+\sin((N-n)\theta)\right]. \end{aligned} \quad \text{(A3)}$$

By employing the relation $\sin(x)\sin(y) = -(1/2)[\cos(x+y) - \cos(x-y)]$ and using Eq. (21),

$$EC_A = -tC_B\frac{\sin(\theta)}{\sin((N+1)\theta)}. \quad \text{(A4)}$$

Analogously, for the $N-n+1$th B-type carbon atom, one can obtain the following relation:

$$\begin{aligned} EC_B\sin((N-n+1)\theta) &= tC_A\left[2\cos\left(\frac{\sqrt{3}}{2}k_x a_{cc}\right)\sin(n\theta)\right. \\ &\left.+\sin((n-1)\theta)\right], \end{aligned} \quad \text{(A5)}$$

which gives

$$EC_B = -tC_A\frac{\sin(\theta)}{\sin((N+1)\theta)}. \quad \text{(A6)}$$

From Eq. (A4) and Eq. (A6), one can find that $C_A = \pm C_B$.

Also, the dispersion relation can be found by multiplying Eq. (A3) by Eq. (A5),

$$\begin{aligned} &E^2 C_A C_B \sin(n\theta)\sin((N-n+1)\theta) \\ &= t^2 C_A C_B\left[4\cos^2\left(\frac{\sqrt{3}}{2}k_x a_{cc}\right)\sin((N-n+1)\theta)\sin(n\theta)\right. \\ &+ 2\cos\left(\frac{\sqrt{3}}{2}k_x a_{cc}\right)\sin((N-n+1)\theta)\sin((n-1)\theta) \\ &+ 2\cos\left(\frac{\sqrt{3}}{2}k_x a_{cc}\right)\sin((N-n)\theta)\sin(n\theta) \\ &\left.+ \sin((N-n)\theta)\sin((n-1)\theta)\right]. \end{aligned} \quad \text{(A7)}$$

With the help of trigonometric identities and Eq. (21), this expression can be reformatted as

$$E = \pm t\left[1 + 4\cos^2\left(\frac{\sqrt{3}}{2}k_x a_{cc}\right) + 4\cos\left(\frac{\sqrt{3}}{2}k_x a_{cc}\right)\cos(\theta)\right]^{1/2}. \quad \text{(A8)}$$

APPENDIX B: CALCULATION OF NORMALIZATION FACTORS

To obtain the normalization factors in the Eq. (3), one has to impose the following condition:[10]

$$\langle\psi_A|\psi_A\rangle = \langle\psi_B|\psi_B\rangle = 1/2. \quad \text{(B1)}$$

By substituting Eq. (15) in Eq. (B1), one obtains

$$\langle\psi_A|\psi_A\rangle = \frac{1}{\Omega}\sum_{n=1}^{N}\left(\sin^2(n\theta)\right) = 1/2. \quad \text{(B2)}$$

It is straightforward to obtain $\Omega_{A/B} = \Omega$ as

$$\begin{aligned} \Omega &= 2\sum_{n=1}^{N}\sin^2(n\theta) = N - \frac{\sin(N\theta)}{\sin(\theta)}\cos((N+1)\theta) \\ &= \frac{1}{2}\left(1 + 2N - \frac{\sin(2N+1)\theta}{\sin(\theta)}\right). \end{aligned} \quad \text{(B3)}$$

In principle, θ cannot be derived analytically for ZGNRs. However, two approximations for θ are discussed. Using Eq. (27), Eq. (B3) can be simplified as

$$\Omega = N + 1/2. \tag{B4}$$

APPENDIX C: RECURSIVE FORMULA SOLUTION

To solve the recursive formula,

$$\phi_{n+1} - C\phi_n + \phi_{n-1} = 0, \tag{C1}$$

one can consider the ansatz $\phi_n = t^n$ and follow the similar equation,

$$t^2 - Ct + 1 = 0. \tag{C2}$$

This equation is the generating polynomial of the recursive formula Eq. (C1). The roots of Eq. (C2) are

$$t_{1,2} = \frac{(C \pm \sqrt{C^2 - 4})}{2}. \tag{C3}$$

The general solution of the difference equation is

$$\phi_n = \alpha t_1^n + \beta t_2^n. \tag{C4}$$

Since t_1 is a root of the equation, the other root, t_2, can be written as $t_2 = t_1^{-1}$.

By substituting those two roots in Eq. (C4), one obtains

$$\phi_n = \alpha t_1^n + \beta t_1^{-n}. \tag{C5}$$

Imposing the initial condition, $\phi_0 = 0$, results in

$$\alpha + \beta = 0, \quad \alpha = -\beta, \tag{C6}$$

and from the Eq. (C5),

$$\phi_n = \alpha(t_1^n - t_1^{-n}). \tag{C7}$$

As a result,

$$\alpha = \frac{\phi_1}{\sqrt{C^2 - 4}}, \quad \beta = -\frac{\phi_1}{\sqrt{C^2 - 4}}. \tag{C8}$$

By substituting Eq. (C3) and Eq. (C8) in Eq. (C7), one obtains

$$\phi_n = \frac{\phi_1}{\sqrt{C^2 - 4}} \left(\frac{C + \sqrt{C^2 - 4}}{2} \right)^n - \frac{\phi_1}{\sqrt{C^2 - 4}} \left(\frac{C - \sqrt{C^2 - 4}}{2} \right)^n. \tag{C9}$$

Eq. (C9) can be rewritten as

$$\phi_n = \frac{\left(\frac{C+\sqrt{C^2-4}}{2}\right)^n - \left(\frac{C-\sqrt{C^2-4}}{2}\right)^n}{\sqrt{C^2 - 4}} \phi_1. \tag{C10}$$

APPENDIX D: OPTICAL MATRIX ELEMENTS

Using Eq. (15) and Eq. (29), the matrix elements $p_{\theta,\theta'}(k_x) \equiv \langle +, \theta, k_x | p_x | -, \theta', k_x \rangle$ for an interband transition from a valence band state $|-, \theta, k_x\rangle$ to a conduction band state $|+, \theta', k_x\rangle$ are obtained as

$$P_{\theta,\theta'} = (x_{\theta'} - x_\theta) \frac{im_0}{\hbar} \langle \theta | H | \theta' \rangle, \tag{D1}$$

$$P_{\theta,\theta'} = \frac{im_0}{\hbar\Omega} \sum_{n=1}^{N} \sum_{m=1}^{N} \left[e^{ik(x_m^B - x_n^A)} \sin(n\theta) \sin(m\theta') \langle A_n | H | B_m \rangle (x_m^B - x_n^A) - e^{ik(x_m^A - x_n^B)} \sin(n\theta') \sin(m\theta) \langle B_n | H | A_m \rangle (x_m^A - x_n^B) \right]. \tag{D2}$$

Considering only the nearest neighbors, each atom with some index, n, has two neighbors with index $N - n + 1$ and one neighbor with index $N - n$ (see Fig. 1). Therefore, the index, m, has only three values, with $\langle A_n | H | B_m \rangle = t$. So we have

$$P_{\theta,\theta'} = \left(\frac{im_0}{\hbar\Omega} \right) \left(\frac{i\sqrt{3} a_{cc} t}{2} \right) \sum_{n=1}^{N} \left[(e^{i\sqrt{3}k_x a/2} - e^{-i\sqrt{3}k_x a/2}) \sin(n\theta) \sin((N - n + 1)\theta') - (e^{-i\sqrt{3}k_x a/2} - e^{i\sqrt{3}k_x a/2}) \sin(n\theta') \sin((N - n + 1)\theta) \right]. \tag{D3}$$

After some algebra and replacing Ω from Eq. (B4), the optical matrix elements are

$$P_{\theta,\theta'} = \frac{-2\sqrt{3} m_0 a_{cc} t}{\hbar(2N + 1)} \sin\left(\frac{\sqrt{3}}{2} k a_{cc} \right) \sum_{n=1}^{N} \left[\sin(n\theta) \sin((N - n + 1)\theta') - \sin(n\theta') \sin((N - n + 1)\theta) \right]. \tag{D4}$$

[1]X. Du, I. Skachko, A. Barker, and E. Andrei, Nat. Nanotechnol. **3**, 491 (2008).
[2]K. Bolotin, K. Sikesb, Z. Jianga, M. Klimac, G. Fudenberga, J. Honec, P. Kima, and H. Stormera, Solid-State Commun. **146**, 351 (2008).
[3]J.-H. Chen, C. Jang, S. Xiao, M. Ishighami, and M. Fuhrer, Nat. Nanotechnol. **3**, 206 (2008).
[4]N. Tombros, C. Jozsa, M. Popinciuc, H. Jonkman, and B. van Wees, Nature (London) **448**, 571 (2008).
[5]S. Cho, Y.-F. Chen, and M. Fuhrer, Appl. Phys. Lett. **91**, 123105 (2007).
[6]M. Freitag, Nat. Nanotechnol. **3**, 455 (2008).
[7]X. Li, L. Zhang, S. Lee, and H. Dai, Science **319**, 1229 (2008).

[8]K. Nakada, M. Fujita, G. Dresselhaus, and M. S. Dresselhaus, Phys. Rev. B **54**, 17954 (1996).
[9]K. Wakabayashi, K. I. Sasaki, T. Nakanishi, and T. Enoki, Sci. Technol. Adv. Mater. **11**, 054504 (2010).
[10]H. Zheng, Z. Wang, T. Luo, Q. Shi, and J. Chen, Phys. Rev. B **75**, 165414 (2007).
[11]R. Saito, G. Dresselhaus, and M. Dresselhaus, *Physical Properties of Carbon Nanotubes* (Imperial College Press, London, 1998).
[12]S. Reich, J. Maultzsch, C. Thomsen, and P. Ordejón, Phys. Rev. B **66**, 035412 (2002).
[13]Y. Hancock, A. Uppstu, K. Saloriutta, A. Harju, and M. J. Puska, Phys. Rev. B **81**, 245402 (2010).
[14]S. V. Goupalov, Phys. Rev. B **72**, 195403 (2005).
[15]P. T. Yu and M. Cardona, *Fundamentals of Semiconductors: Physics and Materials Properties* (Springer, Berlin, 2001).
[16]A. K. Gupta, O. E. Alon, and N. Moiseyev, Phys. Rev. B **68**, 205101 (2003).
[17]G. Dresselhaus and M. S. Dresselhaus, Phys. Rev. **160**, 649 (1967).
[18]T. G. Pedersen, Phys. Rev. B **67**, 113106 (2003).
[19]H. Hsu and L. E. Reichl, Phys. Rev. B **76**, 045418 (2007).